Journal of Alloys and Compounds 504 (2010) 345–350

Contents lists available at ScienceDirect

Journal of Alloys and Compounds

journal homepage: www.elsevier.com/locate/jallcom

Effects of strontium on microstructure and mechanical properties of as-cast Mg–5 wt.%Sn alloy

Hongmei Liu[a], Yungui Chen[b], Haofeng Zhao[c], Shanghai Wei[b], Wei Gao[a,*]

[a] Department of Chemical and Materials Engineering, The University of Auckland, Auckland, New Zealand
[b] School of Materials Science and Engineering, Sichuan University, Chengdu, China
[c] Amorphous and Information Composites Lab, Nanjing University of Information Science & Technology, Nanjing, China

ARTICLE INFO

Article history:
Received 18 February 2010
Received in revised form 21 May 2010
Accepted 29 May 2010
Available online 11 June 2010

Keywords:
Magnesium–tin (Mg–Sn) alloys
Strontium (Sr)
Microstructure
Tensile properties

ABSTRACT

The strontium (Sr) addition to the Mg–5 wt.%Sn alloy results in grain refinement and the formation of a rod-shaped and a bone-shaped MgSnSr intermetallic phase which are mainly straddle on the grain boundaries. The yield strength is improved, while the tensile strength and elongation first increased, and then decreased with a large addition of Sr. Optimum mechanical properties at ambient temperature are obtained at a content of 2.14 wt.%Sr. Tensile properties of the alloys at elevated temperatures are also improved, and the decrease of strength at elevated temperature slowed down with increasing Sr addition, indicating that Sr can improve the thermal stability of Mg–Sn alloys.

1. Introduction

Mg–Sn based alloys were studied in the early 1930s and 1960s [1,2]. After 2000, there has been a renewed interest globally in this alloy system as it has potential applications at elevated temperatures [3–6]. The intermetallic phase Mg_2Sn in Mg–Sn alloys has a much higher melting point (770 °C) than the $Mg_{17}Al_{12}$ phase (462 °C) in Mg–Al alloys [7]. Mg–Sn based alloys are therefore likely to be more creep resistant at elevated temperatures than Mg–Al based alloys. Recent studies on the effects of alloying additions such as Ca, Si, RE on the microstructure and tensile properties and creep resistance of Mg–Sn alloys showed clear improvement of their creep properties [8–10].

Sr is an important alloying element to Mg alloys. It has a grain refinement effect on some Mg alloys such as AZ31 and AZ91 [11,12]. It can also improve room and elevated temperature mechanical properties of Mg alloys, especially the latter [13]. However there are very few reports about the effect of Sr on the Mg–Sn alloys. This paper focuses on the effect of Sr on the microstructure and mechanical properties of as-cast Mg–5 wt.%Sn alloy at ambient and elevated temperatures, exploring a new way to improve the mechanical properties of Mg alloys.

2. Experimental

Four Mg–5 wt.%Sn alloys with Sr addition levels of 0.4, 1.6, 3.2 and 4.8 wt.% were prepared. The composition of Sr has measured by XRF and shown in Table 1.

Pure Mg (99.95 wt.%) and pure Sn (99.98 wt.%) were melted in an MgO crucible under the protection of a RJ-2 flux (composition: 35–41 wt.% $MgCl_2$, 40–43% KCl, 5–11% NaCl, 5–11% $CaCl_2$, 6–12% $BaCl_2$, and <2% MgO). Sr was added as an Mg–40 wt.%Sr master alloy at 730 °C. The melt was stirred to assist dissolution of the master alloy. It was held at 700 °C for 30 min, and then cast into a Cu mould that was preheated up to 250 °C. The cavity dimension is 10 mm × 110 mm × 140 mm.

The tensile tests were conducted at ambient temperature (20 °C) and 175 °C on an electro-universal testing machine (Instron 5569) with a crosshead speed of 2 mm/min. The specimens were cut into slices with an electrical discharge wire. The gauge dimension of each specimen is 7.0 mm × 3.5 mm × 2.0 mm. Six samples of each alloy were tested to obtain one set of mechanical properties.

The metallographic specimens were cut from the same position of each casting. They were polished and etched with a solution of 5 vol.% nitric acid + ethyl alcohol. Quantitative analysis was carried out with linear-intercept method in 50 view fields. Backscatter scanning electron microscopy (BSE) and energy dispersion spectroscopy (EDS) (Philips XL-30S) were performed to identify the intermetallic phases. Differential scanning calorimetry (DSC) was conducted in a METZSCH STA 449C system.

3. Results

3.1. Microstructure

Fig. 1 shows the optical micrographs of four as-cast alloys, exhibiting the grain size became smaller with Sr additions. The dendrite crystals of Mg–5%Sn alloy gradually changed to the equiaxed grain with increasing Sr content. The grain size of the as-cast Mg–5%Sn alloy was ~255 μm [10]. With increasing Sr content from

* Corresponding author. Tel.: +64 9 3737599x88175; fax: +64 9 373 7463.
E-mail address: w.gao@auckland.ac.nz (W. Gao).

0925-8388/$ – see front matter © 2010 Published by Elsevier B.V.
doi:10.1016/j.jallcom.2010.05.156

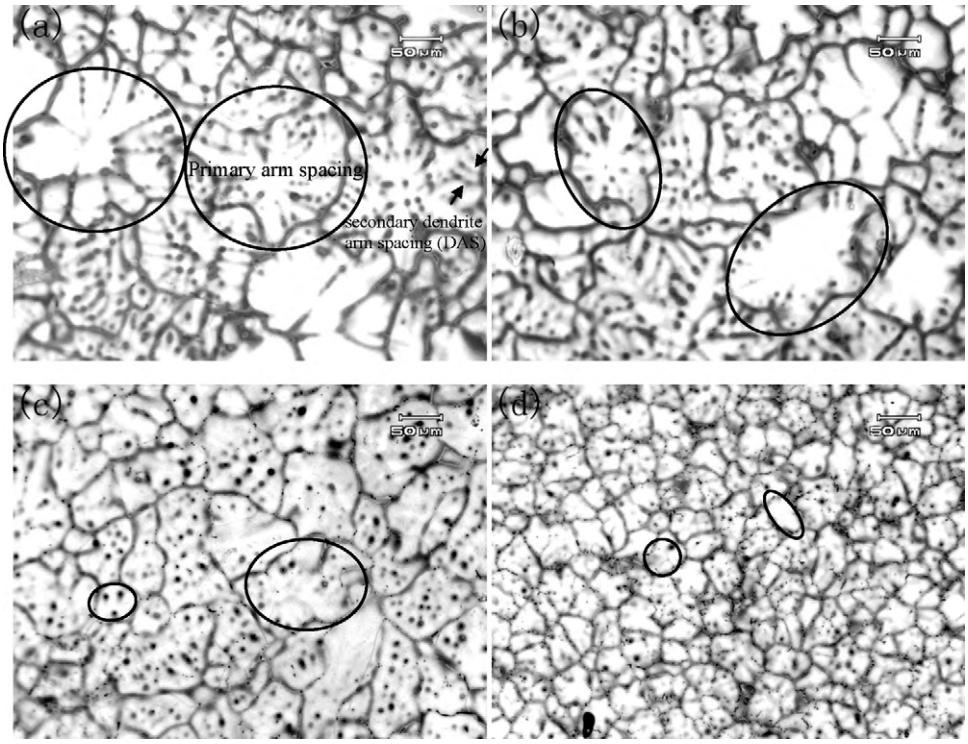

Fig. 1. Optical micrographs of as-cast Mg–5 wt.%Sn–*x*Sr alloys: (a) #1, (b) #2, (c) #3, and (d) #4.

0.29, 1.12, 2.14 and 3.27 wt.%, the primary grain size (marked with circles in Fig. 1) decreased rapidly to 158, 102, 56 and 48 μm.

The addition of Sr to Mg–5%Sn alloy has also led to the formation of new intermetallic phase. The BSE observations supported by the EDS analysis of four alloys are shown in Fig. 2. It can be seen that the α-Mg dendrites in the Sr-containing alloys were refined and the intermetallic Mg_2Sn phase became isolated particles. In addition, a rod-like intermeallic phase was observed (Fig. 2a–d), which was mainly gathered in the grain boundary areas. The volume and size of this phase grew up with the increasing Sr additions. When the

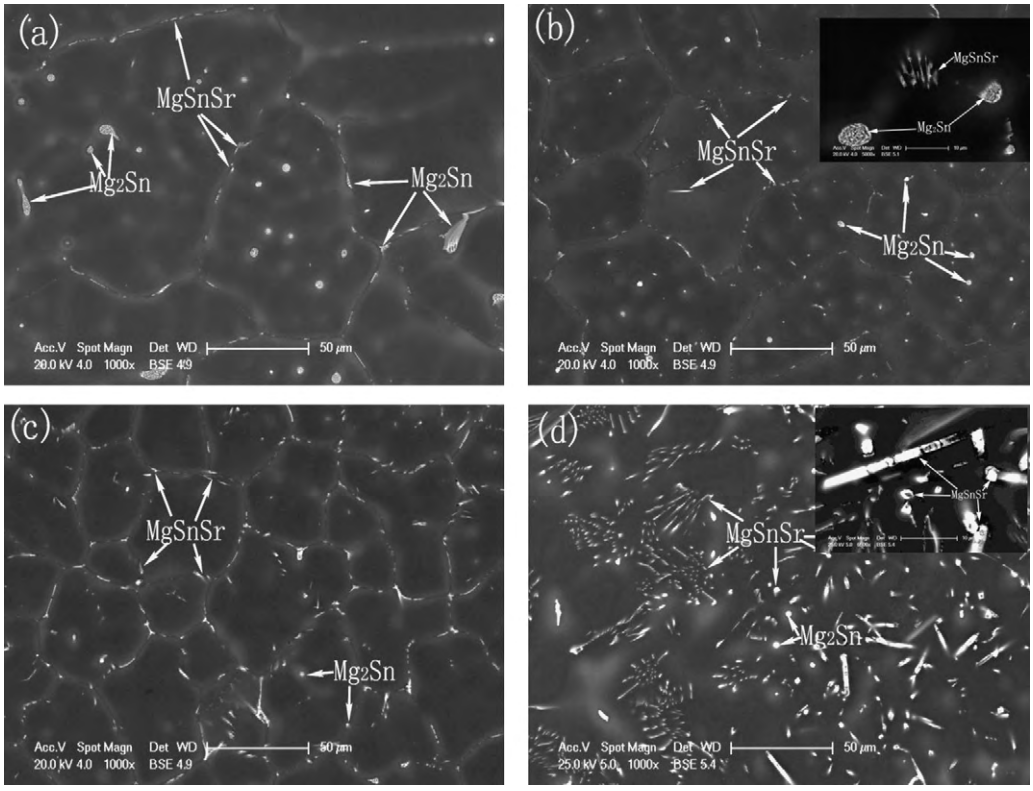

Fig. 2. BSE micrographs of as-cast Mg–5Sn–*x*Sr alloys: (a) #1, (b) #2, (c) #3, and (d) #4.

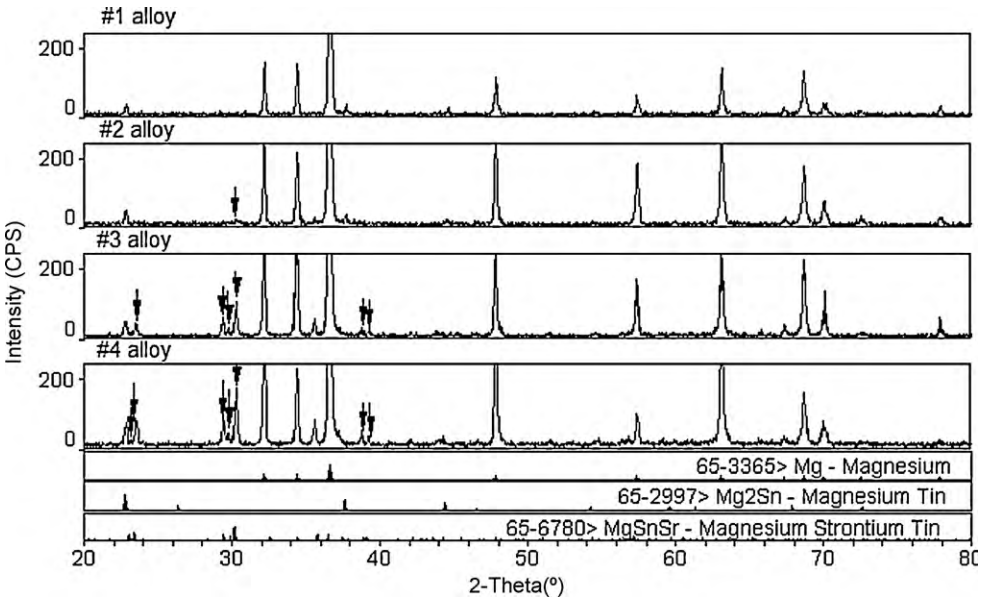

Fig. 3. XRD patterns of Mg–5 wt.%Sn–*x*Sr alloys.

addition of Sr surpassed 2.14 wt.%, some of the rod-like phase grew up to bone-like phase and stretches to the interior of the grains (Fig. 2d). EDS analysis suggested that both rod-like and bone-like were enriched by Sn and Sr with an atomic ratio of Sn:Sr = 1:1.

Fig. 3 shows the XRD patterns obtained for the Mg–5 wt.%Sn alloys with different content of Sr. It can be seen that 1# alloy was primarily composed of α-Mg and Mg_2Sn phases. With increasing Sr content, new diffraction peaks were observed as labeled "↓". The new diffraction peaks perfectly matched the characteristic peaks of MgSnSr, and the MgSnSr phase diffraction peak intensity increased with increasing Sr content, also confirming that the intermetallic phase shown in Fig. 2 was MgSnSr intermetallic compound.

3.2. Mechanical properties

3.2.1. Mechanical properties at ambient temperature

The ambient temperature (~20 °C) tensile properties, including yield strength (YS), ultimate tensile strength (UTS), and elongation for Mg–5%Sn–Sr alloys are shown in Fig. 4a. The results indicated that the YS increased linearly with Sr content, especially when Sr content was over 2.14%. The YS increased by 153% at a 3.27 wt.%Sr content. The UTS and elongation increased firstly and then decreased, reaching an optimum point at a 2.14 wt.%Sr, where the UTS increased by 26% and the elongation by 35%. The UTS and elongation both dropped at 3.27 wt.%Sr content.

3.2.2. Mechanical properties at elevated temperatures.

The results of tensile tests at 175 °C are shown in Fig. 4b. The alloys exhibited lower strengths and higher elongation than that at ambient temperature. However, Table 2 indicates that the decrease of strength became smaller with the increasing Sr addition, indicating that Sr can improve the high temperature tensile strength. Also the UTS and YS values of high Sr containing alloys were quite close compared to that at ambient temperature. #4 alloy had the highest YS but relatively low UTS and elongation (Fig. 4b), while #3 alloy

Table 1
The composition analysis results (wt.%) of studied alloys.

Alloy	Nominal composition	Measured composition (wt.%)		
		Sn	Sr	Mg
#1	Mg–5%Sn–0.4%Sr	4.84	0.29	Bal
#2	Mg–5%Sn–1.6%Sr	4.87	1.12	Bal
#3	Mg–5%Sn–3.2%Sr	4.91	2.14	Bal
#4	Mg–5%Sn–4.8%Sr	4.73	3.27	Bal

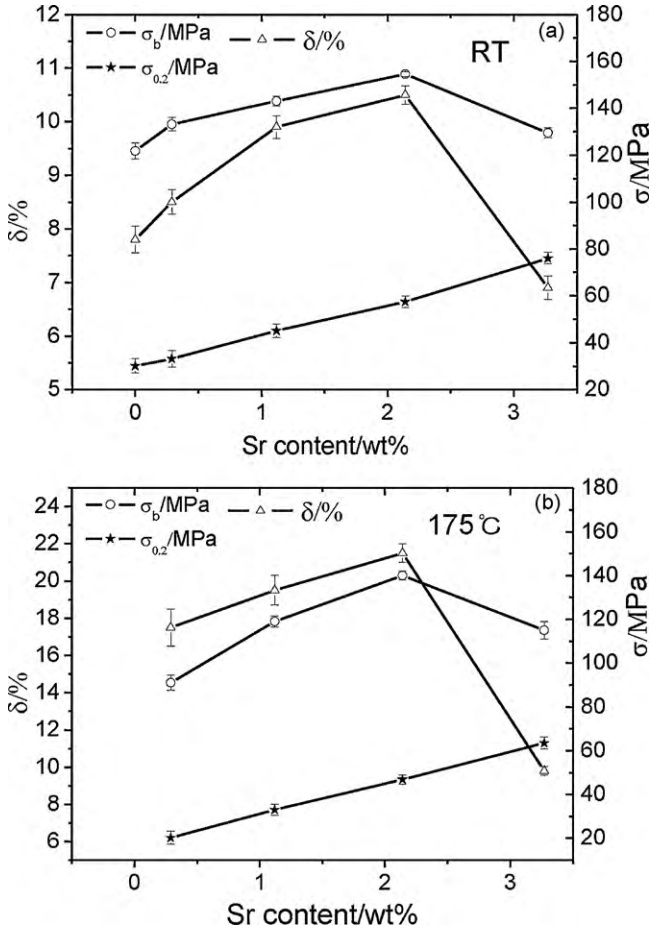

Fig. 4. The effect of Sr on the mechanical properties of Mg–5%Sn alloys at ambient temperature and 175 °C.

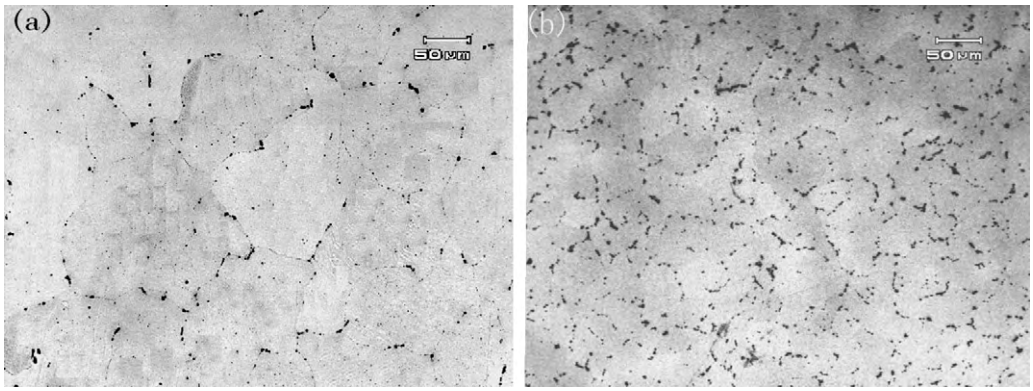

Fig. 5. Optical micrographs of the alloys after a solid-solution treatment at 520 °C for 24 h: (a) #1 and (b) #3 alloys.

Table 2
The decrease (%) of strength at 175 °C from 20 °C.

Alloy	The decreasing ratio (%)	
	$\sigma_{0.2}$	σ_b
#1	41	29
#2	27	12
#3	18	7
#4	12	14

exhibited better overall properties, which followed the same trend of the tensile properties at ambient temperature.

4. Discussion

4.1. The effect of Sr on the ambient temperature mechanical properties

Grain size has an important effect on the mechanical properties of alloys. The addition of Sr to Mg–5%Sn alloy contributes to grain refinement as shown in Fig. 1. Sr forms intermetallic compound $Mg_{17}Sr_2$ and $Mg_{38}Sr_9$ in Mg–Sr master alloy [7]. When adding Sr into Mg–5%Sn alloy, the intermetallic phase dissolves into the melt of Mg–5%Sn alloy. So Sr may be rejected to the front of the solid/liquid interface. Since the solid solubility of Sr in Mg matrix is relatively low (0.11 wt.%), Sr will be enriched in the liquid of growing interface. This may restrict the grain growth during solidification. The grain refinement effect of Sr is believed to relate to the growth restriction effects mechanism (GRE) [12].

On the other hand, the rapid enrichment of solute in the liquid ahead of the growing interface leads to the formation of MgSnSr intermetallic precipitates. It is clearly that the grain size is reduced with the content of Sr increasing up to 3.27 wt.%. It is interesting the formation of Mg–Sn–Sr intermetallic promotes rather than weakens the grain refinement. It shows a somewhat different trend to that in the Mg–Al alloys [14]. Lee et al. [14] investigated the effect of Sr on pure Mg and Mg–Al alloys that showed an effective grain refinement in pure Mg and Mg–1%Al alloy with 0.3%Sr addition and the effect was more pronounced in pure Mg than in Mg–1%Al alloy. When the concentration of Al and Sr increased, the formation of Al_4Sr became more favored, and the grain refining effect decreased or even vanished. They presumed the presence of nucleants formed by a reaction between Mg and Sr, while the formation of Al_4Sr precipitates caused poisoning of nucleants in Mg–Al alloys. The mechanism of grain refinement by Sr has not been well identified [14]. For Mg–Sn alloy, the possibility of nucleation by MgSnSr precipitates should not be excluded, hence whether these particles are suitable for nucleation sites or not needs further study.

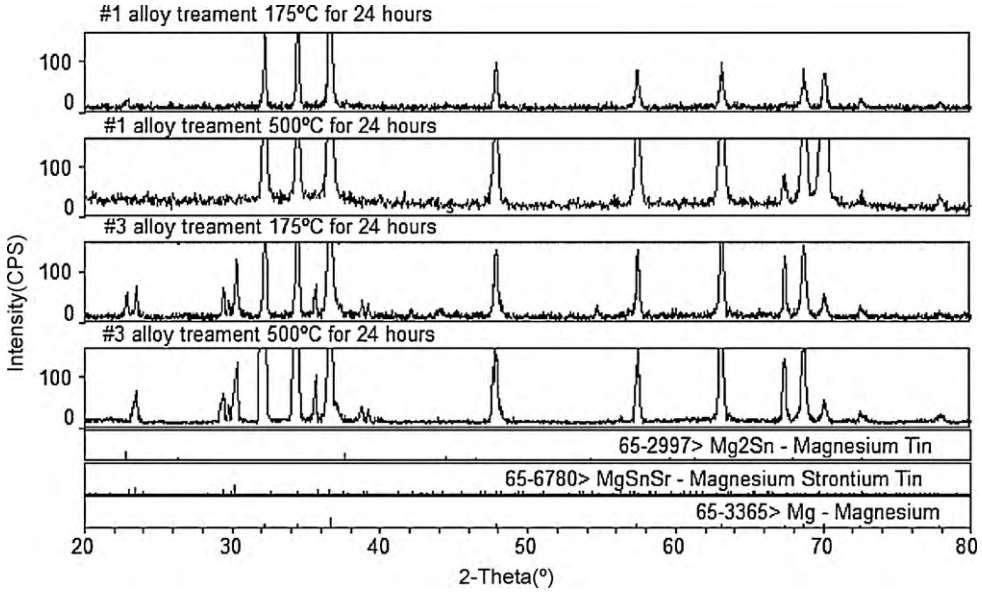

Fig. 6. XRD patterns of #1 and #3 alloy after the treatment at different temperature for 24 h.

The grain refinement by Sr addition improved the tensile properties especially YS. The YS ($\sigma_{0.2}$) can be estimated using the Hall–Petch relations [15,16] as shown in Table 3.

$$\sigma_{0.2} = \sigma_0 + k\sqrt{d}$$

where d is the average grain diameter and k is a constant. For Mg k = 280–320 MPa $\sqrt{\mu m}$ [17]. The value of k is chosen as 300 MPa $\sqrt{\mu m}$, and $\sigma_{0.2}$ (8 MPa) of pure Mg is taken as σ_0 in this calculation. Clearly, the measured results are higher than the calculated values seen in Table 3, and the discrepancy increases with Sr content. This is possibly because that the dispersion strengthening of MgSnSr phases also plays an important role in increasing YS. The discrete MgSnSr particles mainly precipitate along the grain boundary (Fig. 2), which may restrain the movement of dislocations, resulting in extra strengthening effect.

As Sr has a very low solid solubility in the Mg matrix, further addition causes coarsening and volume increasing of MgSnSr phase. Comparing alloy #3 (Fig. 2d) with #4 (Fig. 3e), the quantity of the bone-like phase increased significantly. Meanwhile the volume of Mg_2Sn phase was reduced and the size became smaller. The large intermetallic particles favour the initiation and propagation of cracks under applied stress, leading to the adverse effect on the tensile strength and ductility. This is why even the YS of #4 alloy increased, the UTS and elongation decreased sharply.

4.2. Mechanical properties at elevated temperature

Mg–5%Sn–Sr alloys with Sr additions exhibited the improved tensile properties at elevated temperatures. Intermetallic phases of Mg_2Sn and MgSnSr are effective to increase or keep strengths at elevated temperature since both Mg_2Sn and MgSnSr are quite stable at 175 °C, as shown in Fig. 5 that there is no clearly change of Mg_2Sn and MgSnSr phases after treatment at 175 °C for 24 h. Furthermore, the formation of the rod-shaped MgSnSr phase is more responsible for the increase of strengths at elevated temperature. The decrease of strengths became smaller with the Sr addition, indicating that Sr can improve the high temperature tensile properties. Also the UTS and YS values of high Sr containing alloys are relatively close to that at ambient temperature. After solution treatment for 24 h at 500 °C, the Mg_2Sn phase dissolves into α-Mg matrix but MgSnSr phase has no apparent changes in size or shape, as seen in Fig. 6. DSC curve in Fig. 7 shows that the Mg_2Sn phase dissolves into α-Mg phase at ~406 °C, while the dissolution temperature of MgSnSr is ~555 °C. This confirms that MgSnSr phase has better thermal stability.

For common Mg alloys, grain boundary sliding is the important deformation mechanism at elevated temperatures [18]. The MgSnSr precipitates straddle at the grain boundary areas, with some of them connect into both grains (see Fig. 2d and e), acting as an effective barrier to the mobile sliding system. Sliding of grain boundaries and propagation of cracks are therefore effectively slowed down at elevated temperatures. This microstructure may have more effective influence on the high temperature creep resistance of the alloys, which is currently undergoing tests in our labs.

Table 3
The comparison of YS ($\sigma_{0.2}$) between the calculated values using Hall–Petch relations and measured ones.

Alloys	$\sigma_{0.2}$	
	Calculated	Measured
#1	32.5	33.1
#2	39.8	45.1
#3	49.0	57.5
#4	53.6	76.0

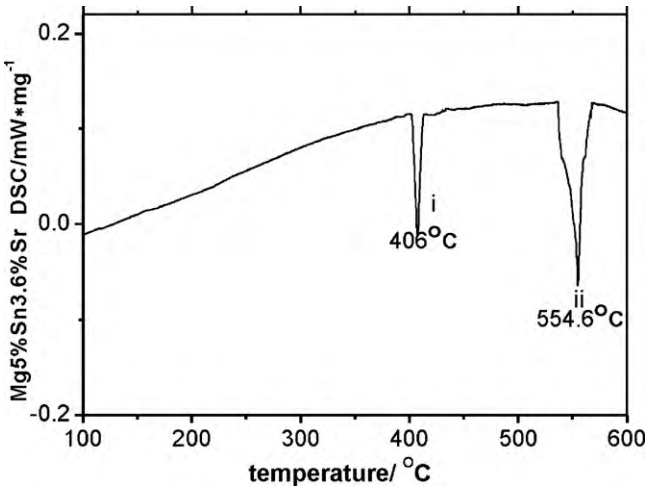

Fig. 7. DSC curves of #3 alloy (3 °C/min).

The change of tensile strength at elevated temperature has the same trends as that at ambient temperature. The number of large bone-shaped MgSnSr particles increases sharply when Sr content is above 2.14 wt.%. The large amount of intermetallic phase is prone to the initiation and propagation of cracks, resulting in the deterioration of the UTS and elongation.

5. Summary and conclusion

(1) The addition of Sr to Mg–5%Sn alloy results in the grain refinement and formation of MgSnSr phase. The morphology of this phase mainly shows a rod-shape morphology when Sr content is below 2.14 wt.% and bone-shape when Sr is above this level. MgSnSr has improved thermal stability than Mg_2Sn.
(2) The addition of Sr improves the yield strength, while the tensile strength and elongation increase first and then decrease with a large addition of Sr. Optimum mechanical properties at the ambient temperature are attained at the content of 2.14 wt.%Sr.
(3) The effect of Sr on the mechanical properties of the alloys at elevated temperature has the same trends as that at ambient temperature. Sr addition improves the thermal stability of Mg–5%Sn alloys.
(4) The improvement of tensile properties at ambient temperature comes from both grain refinement and dispersion strengthening effect of the discrete rod-like MgSnSr phase. The improved tensile properties at elevated temperature are mainly due to the improved thermal stability of the rod-like MgSnSr phase. However, large amount of bone-like MgSnSr phase decreases the UTS and elongation of the alloys.

Acknowledgements

This project is supported by a New Zealand FRST IIOF grant (UoAX 0601). We thank group and Department members especially Mark Taylor, Mike Hodgson, Weiwei Chen and Balan Zhu for assistance.

References

[1] G. Derge, A.R. Kommel, R.F. Mehl, Trans. AIME 124 (1937) 367.
[2] J. Van Der Planken, J. Mater. Sci. 4 (1969) 927–929.
[3] N. Hort, Y. Huang, T.A. Leil, et al., Adv. Eng. Mater. 8 (2006) 359–364.
[4] C.L. Mendis, C.J. Bettles, M.A. Gibson, et al., Mater. Sci. Eng. A 435–436 (2006) 163–171.
[5] T.T. Sasaki, K. Oh-ishi, T. Ohkubo, K. Honoa, Scr. Mater. 55 (2006) 251–254.
[6] S. Cohen, G.R. Goren-Muginstein, S. Avraham, Magnesium Technol. (2004) 301–305.

[7] T.B. Massalski, Binary Alloy Phase Diagrams, ASM International, 1990.
[8] D.H. Kang, S.S. Park, N.J. Kim., Mater. Sci. Eng. A 413–414 (2005) 555–560.
[9] A.L. Bowles, H. Dieringa, C. Blawert, et al., Magnesium Technol. (2004) 307–310.
[10] H. Liu, Y. Chen, Y. Tang, et al., Mater. Sci. Eng. A 464 (2007) 124–128.
[11] H. Liu, Y. Chen, Y. Tang, et al., J. Alloys Compd. 440 (2007) 122–126.
[12] M. Yang, F. Pan, R. Cheng, et al., Mater. Sci. Eng. A 491 (2008) 440–445.
[13] S. Liu, B. Li, X. Wang, W. Su, H. Han, J. Mater. Prod. Technol. 209 (2009) 3999–4004.
[14] Y.C. Lee, A.K. Dahle, D.H. St John., Metall. Mater. Trans. A 31 (2000) 797–895.
[15] E.O. Hall., Proc. Phys. Soc.: Sect. B 64 (1951) 747.
[16] N.J. Petch, J. Iron Steel Inst. 25 (1953) 174.
[17] W. Xiao, S. Jia, J. Wang, Y. Wu, L. Wang, Mater. Sci. Eng. 474 (2008) 317–322.
[18] A.A. Luo., Int. Mater. Rev. 49 (2004) 13–30.